

Adhesion Functions in Cell Sorting by Mechanically Coupling the Cortices of Adhering Cells

Jean-Léon Maître,¹ Hélène Berthoumieux,^{2,3} Simon Frederik Gabriel Krens,¹ Guillaume Salbreux,² Frank Jülicher,² Ewa Paluch,^{4*} Carl-Philipp Heisenberg^{1*}

Differential cell adhesion and cortex tension are thought to drive cell sorting by controlling cell-cell contact formation. Here, we show that cell adhesion and cortex tension have different mechanical functions in controlling progenitor cell-cell contact formation and sorting during zebrafish gastrulation. Cortex tension controls cell-cell contact expansion by modulating interfacial tension at the contact. By contrast, adhesion has little direct function in contact expansion, but instead is needed to mechanically couple the cortices of adhering cells at their contacts, allowing cortex tension to control contact expansion. The coupling function of adhesion is mediated by E-cadherin and limited by the mechanical anchoring of E-cadherin to the cortex. Thus, cell adhesion provides the mechanical scaffold for cell cortex tension to drive cell sorting during gastrulation.

Cell adhesion and cortex tension are commonly assumed to function in cell sorting by controlling cell-cell contact formation (1–5), with adhesion increasing the contact size and cortex tension decreasing it (3–7). To clarify how cell adhesion and cortex tension function in

progenitor cell-cell contact formation and sorting during zebrafish gastrulation, we first developed a mechanical description of two progenitor cells in contact, on the basis of previous models of cell-cell adhesion and sorting (4, 5). The cells are described as fluid objects with a viscoelastic

cortex under tension and adhesive bonds maintaining the cell-cell contact. The size of the cell-cell contact is determined by the balance of forces at the contact boundary:

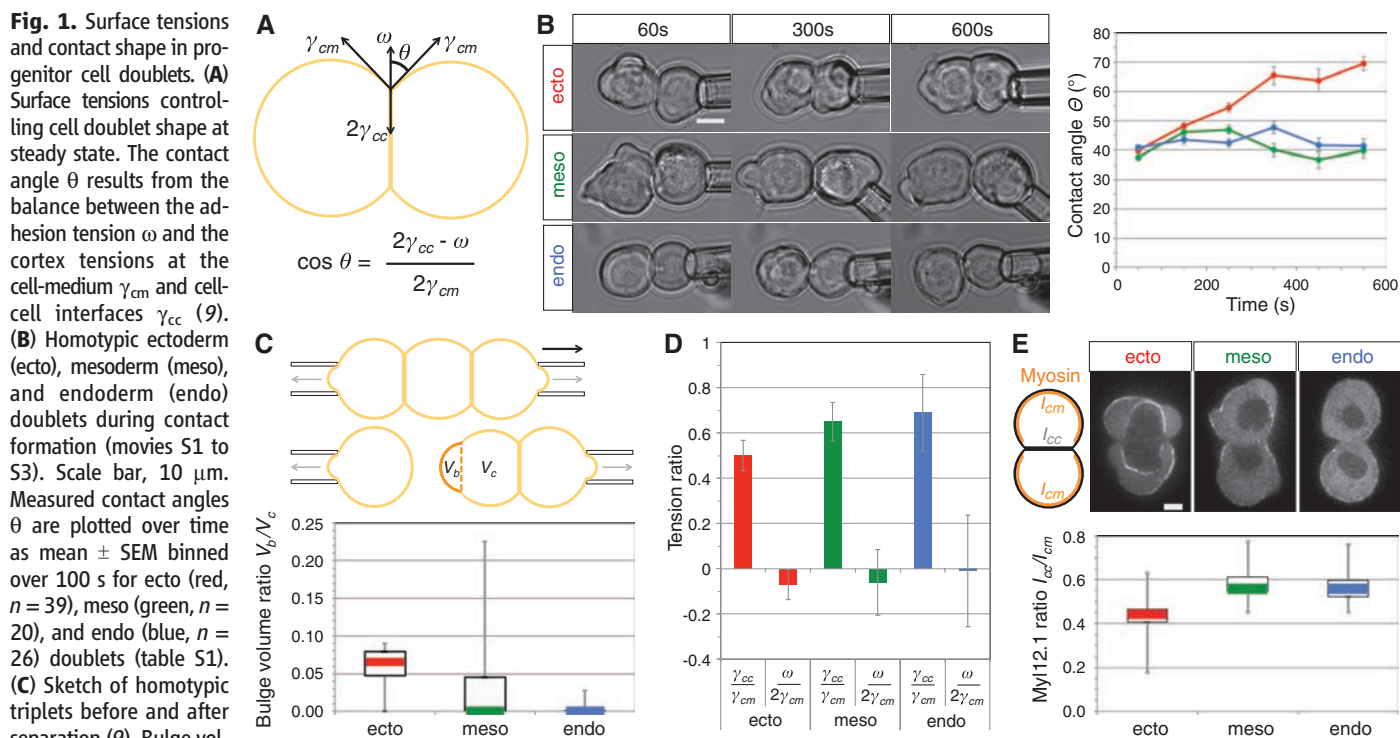
$$\cos(\theta) = \frac{\gamma_i}{2\gamma_{cm}} = \frac{2\gamma_{cc} - \omega}{2\gamma_{cm}} \quad (1)$$

where θ is the contact angle of the two adhering cells (Fig. 1A) (8, 9). The tension γ_i at the cell-cell interface has a positive contribution arising from the cortex tension γ_{cc} of the two cells at the contact and a negative contribution arising from adhesion (adhesion tension) of magnitude ω . Outside of the contact, the tension at the cell-medium interface is equal to the cortex tension γ_{cm} at this interface.

To characterize the mechanical parameters that control progenitor cell-cell contact formation, we first determined the ratio of the

¹Institute of Science and Technology Austria, Klosterneuburg, Austria. ²Max Planck Institute for the Physics of Complex Systems, Dresden, Germany. ³CNRS, Laboratoire de Physique Théorique de la Matière Condensée, UMR 7600, Université Pierre et Marie Curie, Paris, France. ⁴Max Planck Institute of Molecular Cell Biology and Genetics, Dresden, Germany and International Institute of Molecular and Cell Biology, Warsaw, Poland.

*To whom correspondence should be addressed. E-mail: heisenberg@ist.ac.at (C.-P.H.); paluch@mpi-cbg.de (E.P.)



myosin [Myl12.1-eGFP (enhanced green fluorescent protein)] localization in homotypic doublets of pTol2- β -actin::myl12.1-eGFP transgenic zebrafish. Measured mean fluorescence intensity at the cell-cell interface (I_{cc}) is normalized to the mean intensities at the cell-medium interfaces (I_{cm}) of both cells for ecto ($n = 25$), meso ($n = 33$), and endo ($n = 17$) doublets. Scale bar, 5 μ m.

myosin [Myl12.1-eGFP (enhanced green fluorescent protein)] localization in homotypic doublets of pTol2- β -actin::myl12.1-eGFP transgenic zebrafish. Measured mean fluorescence intensity at the cell-cell interface (I_{cc}) is normalized to the mean intensities at the cell-medium interfaces (I_{cm}) of both cells for ecto ($n = 25$), meso ($n = 33$), and endo ($n = 17$) doublets. Scale bar, 5 μ m.

Fig. 2. Contact strength and structure in progenitor cell doublets. **(A)** Separation force F_s of ectoderm (red; $n = 104/41/18$), mesoderm (green; $n = 30/16/11$), and endoderm (blue; $n = 44/23/16$) homotypic doublets is plotted as mean \pm SEM at 1-, 5-, and 10-min contact times (movie S7 and table S4) (9). **(B)** Ratio of separation force F_s to contact radius R_c of ecto ($n = 37$), meso ($n = 15$), and endo ($n = 25$) homotypic doublets after 5-min contact time (table S5). **(C)** Sketch of a cell doublet showing cadherin (purple), actin (cyan), and myosin (orange). Optical sections through cell-cell contacts of homotypic doublets stained with antibodies against Cdh1, Ctnnb1, and Ctnna; phalloidin for F-actin; or expressing Myl12.1-mCherry (fig. S3). Scale bar, 5 μm .

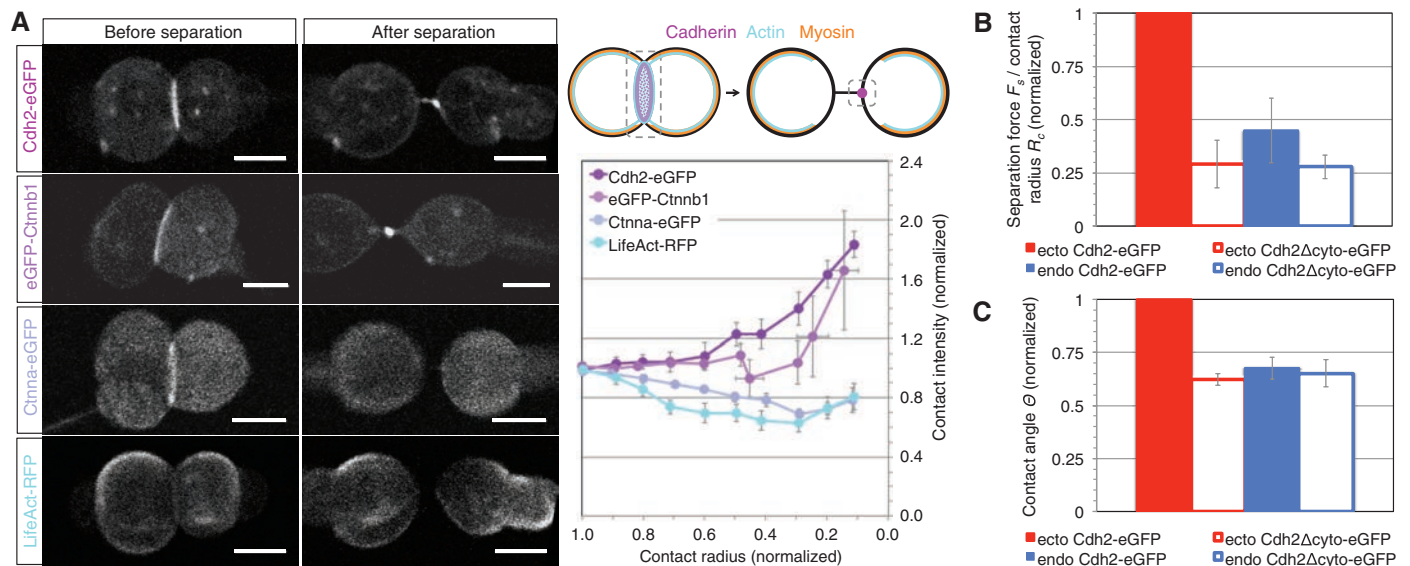
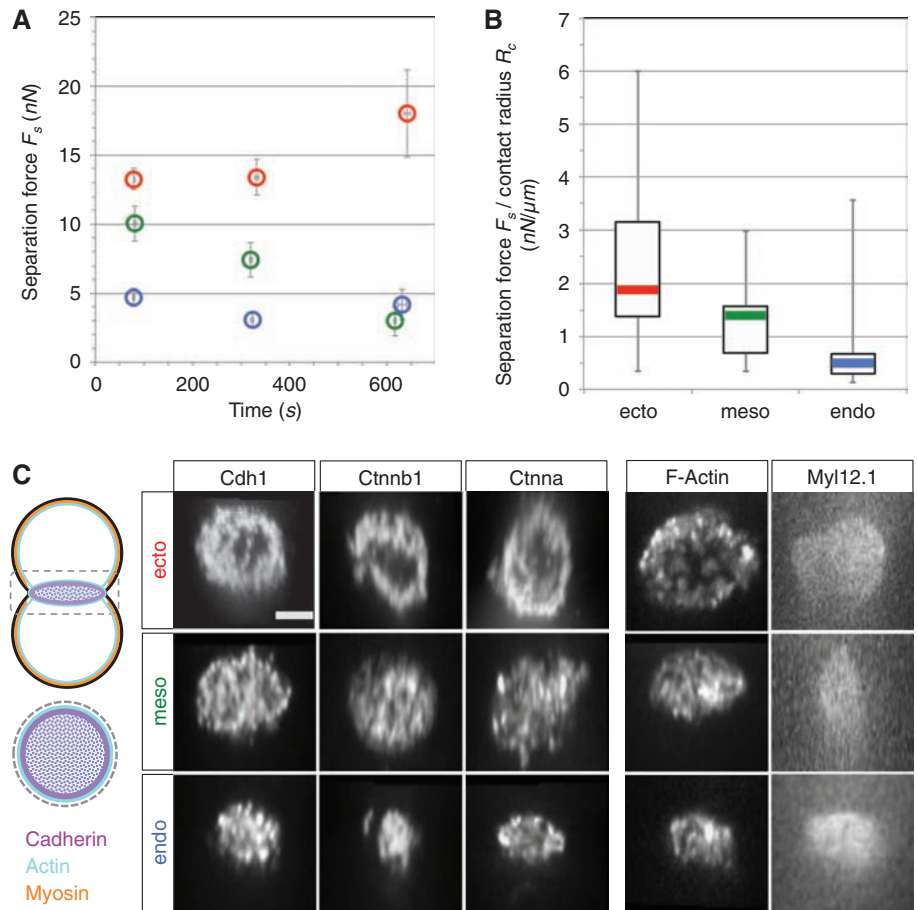


Fig. 3. Cytoskeletal anchoring of Cdh2 in progenitor cell-cell contact formation. **(A)** Ectoderm homotypic doublets expressing Cdh2-eGFP plus LifeAct-RFP (red fluorescent protein) ($n = 15$), eGFP-Ctnnb1 ($n = 20$), or Ctnna-eGFP ($n = 30$) at 5 min contact time before and after separation (movies S8 to S11). Fluorescence intensity at the contact and contact size measured during the separation process (purple and/or cyan on diagram) are plotted as mean \pm SEM relative to the value before the separation

(table S6). Scale bars, 10 μm . **(B and C)** Ratio of separation force to contact radius F_s/R_c (B) or contact angle θ (C) measurements of ectoderm (red) or endoderm (blue) homotypic doublets expressing Cdh2-eGFP ($n = 17/20$) or Cdh2 Δ cyto-eGFP ($n = 20/14$) at 5-min contact time. Values are plotted as mean \pm SEM and normalized to Cdh2 expression level at the measured contact and at the contact of ecto doublets (movies S12 to S15 and tables S7 and S8).

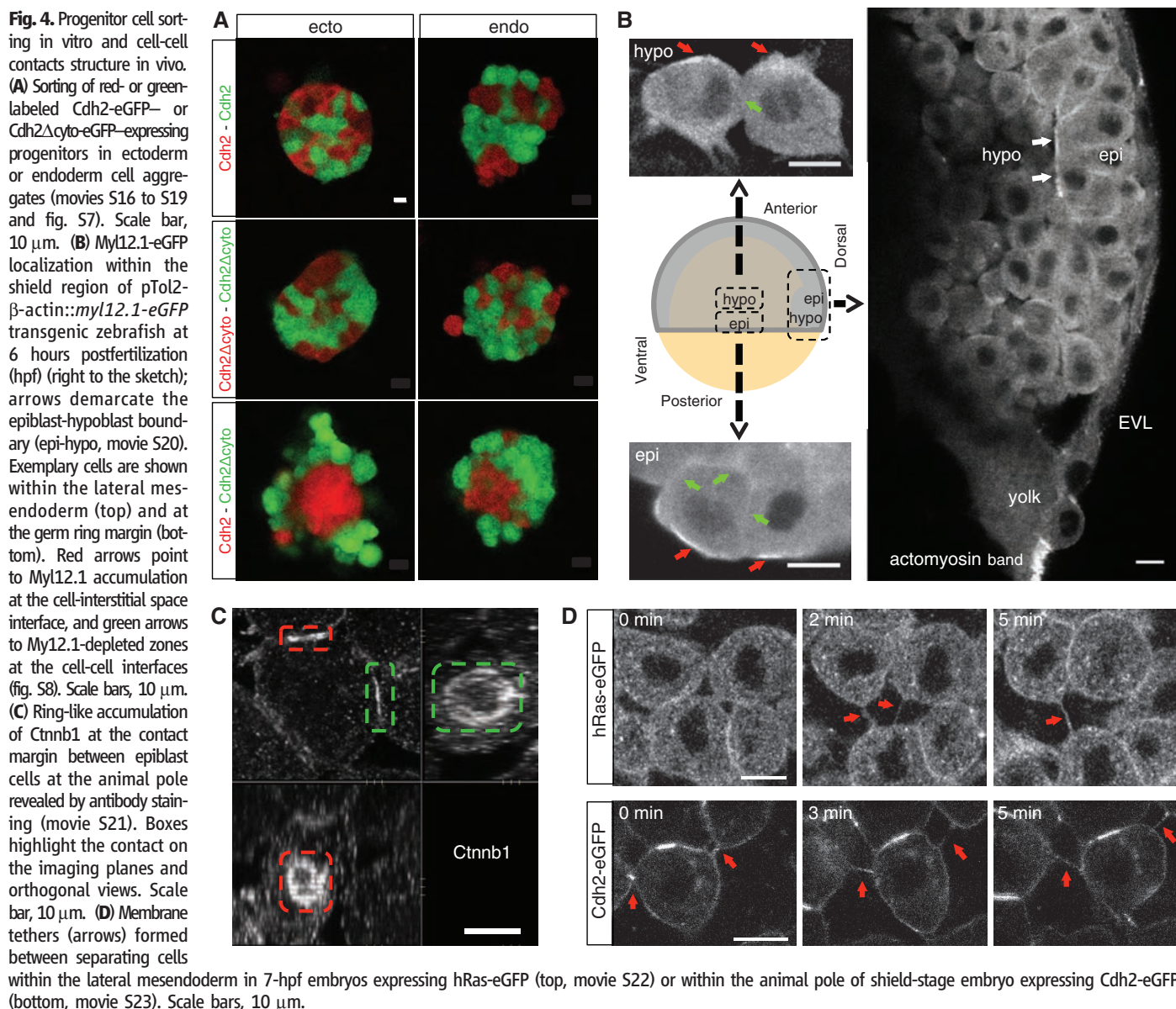
interfacial tensions at the cell-cell and cell-medium interfaces by measuring the contact angle θ of freely adhering cell doublets *ex vivo* and using Eq. 1. Homotypic ectoderm doublets showed a larger contact angle θ and consequently a lower ratio of cell-cell to cell-medium interfacial tensions $\gamma_i/2\gamma_{cm}$ than mesoderm and endoderm doublets (Fig. 1B).

To derive the relative contribution of the cortex tension γ_{cc} and the adhesion tension ω to the ratio of cell-cell to cell-medium interfacial tensions ($2\gamma_{cc} - \omega$)/ $2\gamma_{cm}$, we measured the ratio of cortex tensions at the cell-cell to cell-medium interfaces γ_{cc}/γ_{cm} . To this end, we probed cortex tension at the cell-cell interface by separating contacting progenitor cells *ex vivo*, using a dual pipette aspiration assay (DPA) and analyzing resulting shape changes directly after separation (Fig. 1C). We observed a rapid increase in cur-

vature in the region of the dissolved cell-cell contact, indicative of reduced cortex tension γ_{cc} at this location compared to cortex tension γ_{cm} at the cell-medium interface. To calculate the ratio of cortex tensions γ_{cc}/γ_{cm} from the curvature change at the dissolved cell-cell contact in the different progenitor cell types, we modeled the cell-cell and cell-medium interfaces as elastic shells under tension, consistent with the short time scales of our experiment (9). Using this model, we found γ_{cc}/γ_{cm} to be lower in contacting ectoderm cells compared to mesoderm and endoderm cells (Fig. 1D). Consistent with this, we observed that in progenitor cell doublets, non-muscle myosin-2 (Myl12.1) was reduced at cell-cell compared to the cell-medium interfaces, and that this reduction was more pronounced in ectoderm compared to mesoderm and endoderm doublets (Fig. 1E).

Having determined the ratio of tensions at the cell-cell and cell-medium interfaces, we computed the adhesion tension ω using Eq. 1. We found that for all three progenitor cell types, the magnitude of the adhesion tension ω was considerably smaller than the cortex tension γ_{cc} at the cell-cell interface (Fig. 1D). This indicates that the cell-cell interfacial tension γ_i is dominated by the cortex tension γ_{cc} at this interface. It further suggests that the cell-cell contact angle θ , and thus the contact size, is predominantly controlled by the ratio of cortex tensions γ_{cc}/γ_{cm} between these interfaces and that adhesion tension ω , contrary to previous suggestions (8), has only little function in contact expansion.

Although these findings argue against a critical function of adhesion tension in cell-cell contact expansion, formation of adhesive bonds is still essential to mechanically couple the contractile



cortices of the adhering cells at the contact and to support stresses normal to the adhesion zone arising from cortical tension, intracellular pressure, or external forces (10, 11). Notably, this mechanical coupling of adhesion is distinct from the role adhesion plays in providing the adhesion tension ω , where it acts in the direction tangential to the contact zone, thereby expanding it. To characterize the function of mechanical coupling due to adhesion in progenitor cell-cell contact formation and sorting, we asked how its strength is controlled in the different progenitor cell types, and whether interfering with its strength affects progenitor cell-cell contact formation and cell sorting.

To determine the strength of mechanical coupling due to adhesion, we used the DPA assay to mechanically separate homotypic progenitor cell doublets *ex vivo* and measure the corresponding separation force (12). Considering that cell-cell separation was achieved rapidly (<1 s), our experiments can be described as the separation of two elastic solids, where the separation force F_s depends on different factors, including the number and dissociation rate of adhesion bonds (9, 13). We found that ectoderm doublets exhibit higher F_s at contact times varying from 1 to 10 min than mesoderm and endoderm doublets (Fig. 2A). This difference in F_s between the progenitor cell types is not just a consequence of differences in cell-cell contact size, because normalizing F_s by the contact radius (F_s/R_c) (9) still yielded higher values for ectoderm compared to mesoderm and endoderm doublets (Fig. 2B and fig. S1). Differences in adhesion molecule density at the contact are also unlikely to account for the different F_s , as the expression levels of E-cadherin (Cdh1) and associated proteins, previously shown to mediate adhesion in all three progenitor cell types (1), did not correlate with the different F_s in these cells (fig. S2).

We next asked whether differences in the mechanical resistance of adhesion bonds to pulling forces, previously implicated in controlling F_s (12), are responsible for the differences in F_s between the progenitor cell types. To this end, we first determined whether the binding strength of cadherins across the cell-cell contact or to the cortical cytoskeleton limits their mechanical resistance by analyzing the segregation of adhesion complex components during cell-cell separation. Before separation, Cdh1, β -Catenin (Ctnn1), α -Catenin (Ctnna), and actin, but not Myl12.1, were found to accumulate in a dense ring-like structure at the margin of the cell-cell contact in ectoderm and, to a lesser extent, mesoderm and endoderm doublets (Fig. 2C and figs. S3 and S4). This suggests that higher F_s values coincide with adhesion molecules accumulating at the contact edge. Upon separation by means of the DPA, progenitor cells remained connected via long plasma membrane tethers, and N-cadherin (Cdh2; see below for using Cdh2 as a proxy for Cdh1) together with Ctnn1, which directly binds to Cdh2 (10),

accumulated in these tethers (Fig. 3A). By contrast, Ctnna, which directly or indirectly couples Ctnn1 to the actin cytoskeleton (14, 15), did not colocalize with Cdh2 and Ctnn1 in the tethers, but instead disassembled from the dissolving cell-cell contact together with actin (Fig. 3A). These findings indicate that cadherins dissociate from the cytoskeleton during progenitor cell separation, suggesting that cytoskeletal anchoring of cadherins limits the mechanical resistance of adhesion bonds to pulling forces.

To explore whether modifying cytoskeletal anchoring of cadherins, and thus the mechanical resistance of adhesion bonds to pulling forces, affects F_s and cell-cell contact formation, we expressed either a full-length version of Cdh2 or a truncated version of Cdh2 that cannot bind to the cortical cytoskeleton (Cdh2 Δ cyto) (12) in progenitor cells deprived of endogenous Cdh1 expression (cdh1 morphant cells). Expressing similar levels of Cdh2 in homotypic ectoderm and endoderm cell doublets changed neither their endogenous relative difference in F_s normalized by the contact radius F_s/R_c nor their contact angle θ . However, expressing Cdh2 Δ cyto strongly reduced F_s/R_c and θ to similar low levels in both cell types (Fig. 3, B and C, and figs. S5 and S6). This suggests that proper cytoskeletal anchoring of cadherins is an essential factor determining the difference in separation force and cell-cell contact size between the progenitor cell types.

We next asked how far the observed effect of cadherin cytoskeletal anchoring on F_s/R_c and θ influences progenitor cell sorting. Consistent with a critical function of cell-cell contact formation in cell sorting, replacing endogenous Cdh1 with either full-length or truncated Cdh2 in homotypic ectoderm or endoderm progenitor cell aggregates led to cells expressing Cdh2 being sorted into the middle, surrounded by cells expressing Cdh2 Δ cyto (Fig. 4A). These observations suggest that proper cytoskeletal anchoring of cadherins is essential for progenitor cell sorting.

To address how our observations of cell doublets *ex vivo* relate to the situation within the gastrulating embryo, we asked whether progenitor cells segregate *in vivo* by using the same cell-cell contact formation strategies as their counterparts *ex vivo*. Analysis of the cell cortex in germ layer progenitor cells *in vivo* showed that similar to what we observed *ex vivo*, cortical Myl12.1 was preferentially located at cell-interstitial space/extracellular matrix interfaces (Fig. 4B). This suggests that cortex tension is reduced at cell-cell interfaces both *ex vivo* and *in vivo*. Moreover, analysis of progenitor cell-cell contacts *in vivo* revealed a ring-like localization of adhesion molecules reminiscent of the situation in cell doublets *ex vivo* (Fig. 4C). Finally, progenitor cells separating *in vivo* often formed membrane tethers at their dissolving contacts containing Cdh2 (Fig. 4D), similar to cell doublets *ex vivo* that were separated by means of

the DPA. These marked similarities between the situations *ex vivo* and *in vivo* suggest that progenitor cell sorting *in vivo* is driven by the same mechanisms of cell-cell contact formation as observed *ex vivo*.

The mechanical coupling function of cadherins at the cell-cell contact critically requires sufficient anchoring of cadherins to the cortical cytoskeleton. Considering that mechanical load on cadherin adhesion complexes has previously been suggested to modify its cytoskeletal anchoring strength (15, 16), it is intriguing to speculate that this anchoring strength in the different progenitor cell types is determined by the cortex tension of these cells pulling on the mechano-sensitive adhesion complexes, thereby setting their anchoring strength.

References and Notes

1. M. Krieg *et al.*, *Nat. Cell Biol.* **10**, 429 (2008).
2. J. Käfer, T. Hayashi, A. F. Marée, R. W. Carthew, F. Graner, *Proc. Natl. Acad. Sci. U.S.A.* **104**, 18549 (2007).
3. T. Hayashi, R. W. Carthew, *Nature* **431**, 647 (2004).
4. G. W. Brodland, *J. Biomech. Eng.* **124**, 188 (2002).
5. M. L. Manning, R. A. Foty, M. S. Steinberg, E.-M. Schoetz, *Proc. Natl. Acad. Sci. U.S.A.* **107**, 12517 (2010).
6. C. Bertet, L. Sulak, T. Lecuit, *Nature* **429**, 667 (2004).
7. R. A. Foty, M. S. Steinberg, *Dev. Biol.* **278**, 255 (2005).
8. J.-L. Maître, C.-P. Heisenberg, *Curr. Opin. Cell Biol.* **23**, 508 (2011).
9. Information on materials and methods is available on Science Online.
10. A. C. Martin, M. Gelbart, R. Fernandez-Gonzalez, M. Kaschube, E. F. Wieschaus, *J. Cell Biol.* **188**, 735 (2010).
11. N. Borghi *et al.*, *Proc. Natl. Acad. Sci. U.S.A.* **109**, 12568 (2012).
12. Y. S. Chu *et al.*, *J. Cell Biol.* **167**, 1183 (2004).
13. U. Seifert, *Phys. Rev. Lett.* **84**, 2750 (2000).
14. S. Yamada, S. Pokutta, F. Drees, W. I. Weis, W. J. Nelson, *Cell* **123**, 889 (2005).
15. Q. le Duc *et al.*, *J. Cell Biol.* **189**, 1107 (2010).
16. S. Yonemura, Y. Wada, T. Watanabe, A. Nagafuchi, M. Shibata, *Nat. Cell Biol.* **12**, 533 (2010).

Acknowledgments: We thank M. Biro, J.-Y. Tinevez, and J. Rönsch for technical assistance, V. Barone for critical reading of earlier versions of this manuscript, and the facilities of the MPI-CBG and IST Austria for their continuous support. This work was supported by the Max-Planck-Society and grants from the Polish Ministry of Science and Higher Education to E.P. (454/N-MPG/2009/0), the Human Frontier Science Program to E.P. (RGY0067/2008), and the Fonds zur Förderung der wissenschaftlichen Forschung (FWF) to C.-P.H. (HE3231/6; I812-B12).

Supplementary Materials

www.sciencemag.org/cgi/content/full/science.1225399/DC1
Supplementary Text

Materials and Methods

Figs. S1 to S10

Tables S1 to S12

References

Movies S1 to S23

30 May 2012; accepted 1 August 2012

Published online 23 August 2012;

10.1126/science.1225399